Nuclear Instruments and Methods in Physics Research B 410 (2017) 200–206

Contents lists available at ScienceDirect

Nuclear Instruments and Methods in Physics Research B

journal homepage: www.elsevier.com/locate/nimb

Modeling thermal spike driven reactions at low temperature and application to zirconium carbide radiation damage

Christopher J. Ulmer *, Arthur T. Motta

Department of Mechanical and Nuclear Engineering, The Pennsylvania State University, University Park, PA 16802, USA

ARTICLE INFO

Article history:
Received 14 June 2017
Received in revised form 14 August 2017
Accepted 14 August 2017

Keywords:
Rate theory
Ion irradiation
Zirconium carbide
Thermal spike
Athermal

ABSTRACT

The development of TEM-visible damage in materials under irradiation at cryogenic temperatures cannot be explained using classical rate theory modeling with thermally activated reactions since at low temperatures thermal reaction rates are too low. Although point defect mobility approaches zero at low temperature, the thermal spikes induced by displacement cascades enable some atom mobility as it cools. In this work a model is developed to calculate "athermal" reaction rates from the atomic mobility within the irradiation-induced thermal spikes, including both displacement cascades and electronic stopping. The athermal reaction rates are added to a simple rate theory cluster dynamics model to allow for the simulation of microstructure evolution during irradiation at cryogenic temperatures. The rate theory model is applied to in-situ irradiation of ZrC and compares well at cryogenic temperatures. The results show that the addition of the thermal spike model makes it possible to rationalize microstructure evolution in the low temperature regime.

1. Introduction

The degradation of material properties is one of several limiting factors in nuclear reactor performance. This process occurs, in part, by microstructural and microchemical changes induced by irradiation, and prediction of microstructure evolution is necessary as part of an accurate prediction of future material performance in a reactor environment. Rate theory is a method by which microstructure evolution under irradiation is modeled [1–3]. Similar to chemical rate theory, systems of equations involving species' concentrations and reaction rates are solved to yield defect cluster concentrations. Reactions are generally controlled by diffusion of the reactants and are, as such, dependent on temperature.

A simple rate theory approach is to consider the equal production of interstitials and vacancies with the only allowable reaction being the mutual annihilation of those species by recombination. In that regime $C_i = C_v = C$ and the governing equation for this system is

$$\frac{\partial C}{\partial t} = G - RC^2 \tag{1}$$

where C is the concentration of interstitials and vacancies, G is the rate of production of interstitials and vacancies, and R is the rate constant for recombination with the term RC^2 being the rate of recombination. The analytical solution for this equation is

$$C(t) = \sqrt{\frac{G}{R}}\tanh\left(\sqrt{GR}t\right) \tag{2}$$

and describes a system in which the concentrations of interstitials and vacancies increase until being limited by mutual recombination at $C = \sqrt{G/R}$ after a time $t = 1/\sqrt{GR}$. This system is referred to as recombination-dominated.

Reactions in the rate theory framework are typically diffusion-controlled. The rate constant R is therefore proportional to the diffusion coefficients of the reactants. Because of this, as the temperature decreases, so do the diffusion coefficients which causes the steady-state defect concentration, $C = \sqrt{G/R}$, to increase. For the rate constant R defined as in Eq. (17), and for reasonable values of the relevant properties in ZrC, the steady-state atomic concentration of interstitials and vacancies is on the order of 10^{-5} at 300 K. For the same parameters at 50 K, however, the concentration of defects is unphysically $\gg 1$, indicating that the high temperature model is no longer valid. The defect concentration at room temperature, while high, is within reason, but the concentration at 50 K is completely non-physical.

This demonstrates a fundamental limitation of the typical rate theory approach: classical rate theory does not model the microstructure evolution at low temperatures in any meaningful

* Corresponding author.
E-mail address: cju5002@psu.edu (C.J. Ulmer).

http://dx.doi.org/10.1016/j.nimb.2017.08.015
0168-583X/

way. The same is true for more complex systems where individual defects can agglomerate into defect clusters, such as dislocation loops and voids. At very low temperatures, the slow diffusion controlled reactions would inhibit the nucleation and growth of defect clusters in the rate theory framework.

In-situ irradiation of ZrC was previously performed at temperatures ranging from 20 K to 1073 K [4]. The observed microstructure evolution did not vary greatly over the temperature range of 20 K to room temperature; small "black-dot" defects appeared after an incubation dose and their density increased until saturation without growing to form distinct dislocation loops. The black-dot defects are clusters with size estimated on the order of tens of individual defects. The presence of an incubation dose indicates that the defects resolvable by transmission electron microscopy (TEM) were not produced *directly* in single displacement cascades but, rather, formed over time during irradiation. At 20 K, a slow accumulation of defects into larger aggregates by thermal diffusion is not viable given the low defect diffusion coefficient at these temperatures [5], thus another process is required to explain these results.

In this work, we present an addition to rate theory which relies on the defect mobility within displacement cascades. In particular, the thermal spike model of Vineyard [6] is used to calculate an "athermal", radiation-driven component for each reaction rate that is effective even at cryogenic temperatures. This baseline irradiation response can then be added to the usual thermally activated processes to model the reactions at all temperatures. The new reactions are applied to basic ZrC rate theory for evaluation, and these results are reviewed in the context of the experimental measurements of average defect diameter and density as functions of dose. Further recommendations for improving the model are provided.

2. Athermal reaction rates

Atomic collisions with energetic ions transfer energy to lattice atoms during ion irradiation. In this model, this deposited energy drives reactions even at low ambient temperature through defect mobility within the cascade, as put forward by Vineyard [6]. Following Vineyard, the initial collision is considered as an instantaneous point-source of heat. The heat then thermally diffuses outwardly in the radial direction of a spherically symmetric system. The local temperature increase due to the addition of heat by the collision results in a number of atomic jumps which cause reactions that would not otherwise occur at these temperatures. For ion irradiation, additional electronic stopping is considered as an instantaneous line-source of heat. This heat instead diffuses outwardly in the radial direction of a cylindrically symmetric system.

The thermal spike model is applied to diffusion controlled reactions. Being diffusion controlled, the reaction rate density takes the form

$$(\text{rate})_{\text{diff}} = A\exp(-E/(k_B T)) \tag{3}$$

where A is a constant, E is the energy barrier, k_B is the Boltzmann constant, and T is the temperature. For a homogeneous medium with constant thermal conductivity and heat capacity, the heat equation is solved with solutions [6]

$$T_s(r,t) = \left(\frac{qC^{1/2}}{(4\pi\kappa t)^{3/2}}\right)\exp\left(\frac{-Cr^2}{4\kappa t}\right) \tag{4}$$

for the spherical thermal spike and

$$T_c(r,t) = \left(\frac{\epsilon}{4\pi\kappa t}\right)\exp\left(\frac{-Cr^2}{4\kappa t}\right) \tag{5}$$

for the cylindrical thermal spike, where r is the radial distance from the center of the thermal spike, t is the time from the initiation of the thermal spike, q is the energy of the spherical thermal spike, ϵ is the energy deposited per unit line length in the cylindrical thermal spike, κ is the thermal conductivity of the material, and C is the heat capacity of the material. The total number of reactions resulting from the thermal spikes, η, is calculated by integrating the reaction rate density over the whole thermal spike with

$$\eta_s = \int_0^\infty 4\pi r^2 dr \int_0^\infty A\exp(-E/(k_B T))dt = A\left(\frac{\sqrt{3/5}\,\Gamma(5/3)q^{5/3}}{10\pi\kappa C^{2/3}(E/k_B)^{5/3}}\right) \tag{6}$$

for spherical thermal spikes and

$$\eta_c = \int_0^\infty 2\pi r dr \int_0^\infty A\exp(-E/(k_B T))dt = A\left(\frac{\epsilon^2}{8\pi\kappa C(E/k_B)^2}\right) \tag{7}$$

for cylindrical thermal spikes, where $\Gamma(5/3)$ is the gamma function evaluated at 5/3.

The rate of reactions resulting from thermal spikes is then calculated from the results of Eqs. (6) and (7). The number of reactions resulting from a spherical cascade is calculated using the average collision energy, the result of which is then multiplied by the number of collisions per unit volume and time, φ. The number of reactions per unit line length is calculated using the average electronic stopping power and is then multiplied by the ion flux, ϕ. The average spherical thermal spike energy is calculated as the average of all SRIM cascade energies weighted to the 5/3 power, and the average cylindrical thermal spike energy is the electronic stopping power averaged over the thickness of the thin-foil. The final result for the thermal spike reaction rate density follows as

$$(\text{rate})_{\text{spike}} = \eta_s\varphi + \eta_c\phi = A\left[\frac{\sqrt{3/5}\,\Gamma(5/3)\overline{q^{5/3}}\varphi}{10\pi\kappa C^{2/3}(E/k_B)^{5/3}} + \frac{\overline{\epsilon^2}\phi}{8\pi\kappa C(E/k_B)^2}\right] \tag{8}$$

such that the temperature-dependent exponential term of Eq. (3) is replaced by a term evaluated using a combination of material properties and irradiation parameters.

The material properties needed to evaluate Eq. (8) are found in the literature, and the irradiation parameters were specifically evaluated for this work. The Stopping and Range of Ions in Matter (SRIM) [7] is a Monte Carlo program commonly used to simulate ion irradiation, and it was used while planning the in-situ irradiation experiments of ZrC to find the relationship between damage level in displacements-per-atom (dpa) and ion fluence. In this simulation, the average displacement cascade energy was found to be 9361 eV, and the number of cascades per ion was extracted from the text-based collision details. These parameters are used to define the spherical thermal spikes. The average electronic stopping power, 1100 eV nm^{-1}, was estimated from the SRIM graphical user interface ionization plot. This is used to define the cylindrical thermal spike.

The total reaction rate is defined as the sum of the thermal diffusion reaction rate and the thermal spike reaction rate.

$$\begin{aligned}(\text{rate}) &= (\text{rate})_{\text{diff}} + (\text{rate})_{\text{spike}} \\ &= A\left[\exp(-E/(k_B T)) + \frac{\sqrt{3/5}\,\Gamma(5/3)\overline{q^{5/3}}\varphi}{10\pi\kappa C^{2/3}(E/k_B)^{5/3}} + \frac{\overline{\epsilon^2}\phi}{8\pi\kappa C(E/k_B)^2}\right]\end{aligned} \tag{9}$$

The behavior of this new formula is easily understood from inspection. At very low temperatures, $T \ll (E/k_B)$, the thermal diffusion term approaches zero and only the thermal spike reaction rate remains. At higher temperatures, both the thermal diffusion

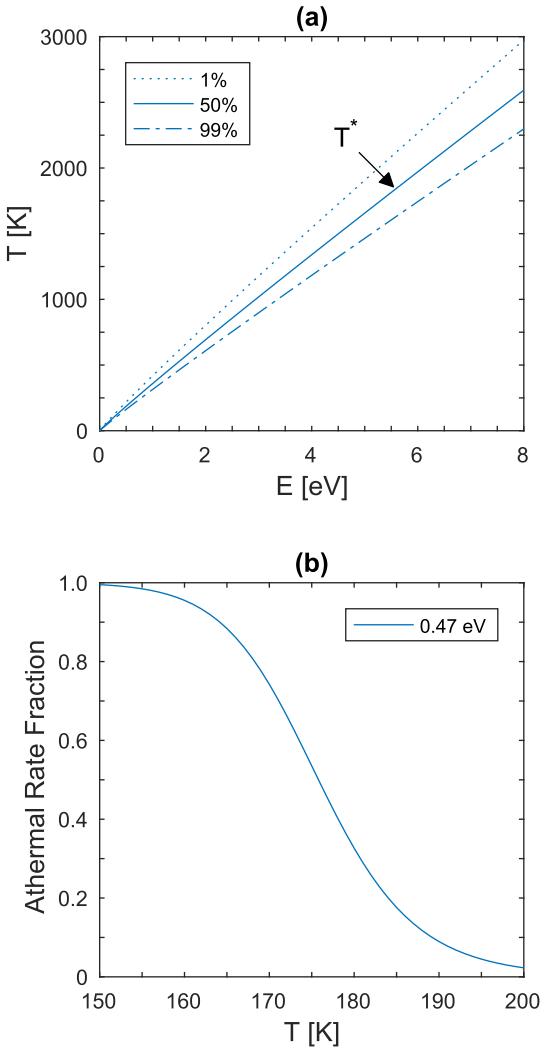

Fig. 1. (a) The temperatures at which the "athermal" thermal spike reaction rate contributes 99%, 50%, and 1% of the total reaction rate for reaction energy E. (b) The athermal reaction rate fraction of the total reaction rate as a function of temperature for 0.47 eV reaction energy, Zr interstitial migration in ZrC.

reaction rate and thermal spike reaction rate contribute. Comparing the thermal diffusion reaction rate of Eq. (3) with the thermal spike reaction rate of Eq. (8), there exists a temperature at which the two reaction rates have equal magnitude, T^*.

$$T^* = -\frac{E}{k_B}\left[\ln\left(\frac{\sqrt{3/5}\,\Gamma(5/3)\overline{q^{5/3}}\varphi}{10\pi\kappa C^{2/3}(E/k_B)^{5/3}} + \frac{\overline{\epsilon^2}\phi}{8\pi\kappa C(E/k_B)^2}\right)\right]^{-1} \tag{10}$$

Above this temperature, the thermal diffusion reaction rate contributes the majority of the total reaction rate, and below this temperature the "athermal" thermal spike reaction rate contributes the majority of the total reaction rate. The equivalent temperature is plotted as a function of reaction energy in Fig. 1 (a) for the in-situ irradiation of ZrC using the parameter values listed in Table 1. Additionally, lines denoting 1% and 99% athermal contribution to the total reaction rate are included. For reactions controlled by interstitial migration of Zr in ZrC ($E_{mi} = 0.47$ eV), the results indicate that the reaction rate for thermal spikes becomes dominant below 176 K. The athermal fraction of the total reaction rate is shown for these reactions as a function of temperature in Fig. 1(b). The transition from the athermal to the thermal regime is nearly completed in the temperature range of 150 K to 200 K.

3. ZrC rate theory model

As reported previously [4,8], the dynamics of ZrC microstructure evolution under irradiation are thought to be controlled by the Zr sublattice such that the visible defects are inferred to be zirconium interstitial clusters. This is because anti-site defects are energetically unfavorable [9], and the high concentration of structural vacancies on the carbon sublattice would suppress the build-up of carbon interstitials. Additionally, the migration energy for zirconium vacancies is too high for cluster growth to occur at the low temperatures it is observed. Therefore, this model considers only Zr vacancies and interstitials and clusters of each defect. In addition, only point defects, Zr interstitials and vacancies, are produced during irradiation, and only these point defects are mobile. This is done for simplicity and also because not much information is known on defect cluster mobility and defect cluster production in displacement cascades in ZrC.

Table 1
Rate theory model parameters.

Zr interstitial formation energy	E_{fi}	8.72	eV	[9]
Zr interstitial migration energy	E_{mi}	0.47	eV	[5]
Zr interstitial diffusion prefactor	D_{0i}	2.2×10^{-7}	m^2/s	
Zr vacancy formation energy	E_{fv}	7.19	eV	[9]
Zr vacancy migration energy	E_{mv}	5.44	eV	[5]
Zr vacancy diffusion prefactor	D_{0v}	1.1×10^{-6}	m^2/s	
Displacement rate	G	1.3×10^{-3}	dpa/s	
Defect survival fraction	χ	0.4		
Sample thickness	L	100	nm	
Atomic volume	Ω	2.596×10^{-29}	m^3	
Interstitial bias		1.05		
Ion flux	ϕ	6.25×10^{15}	$ions/m^2s$	
Displacement cascade rate	φ	6.36×10^{24}	$1/m^3s$	
Average displacement cascade energy	q	9361	eV	
Average electronic stopping power	ϵ	1100	eV/nm	
Thermal conductivity	κ	25	W/(m K)	[14]
Heat capacity	C	3.2×10^6	$J/(m^3K)$	[14]
Di-interstitial binding energy	$E_{bi}(2)$	1.2	eV	[8]
Di-vacancy binding energy	$E_{bv}(2)$	0.25	eV	[8]
Recombination radius	r_c	2.714×10^{-10}	m	

The defect reactions considered in this model include the following: 1. recombination when point defects of opposite nature combine to reform the perfect lattice, 2. formation of a defect cluster when point defects of the same nature react to create a larger cluster, 3. growth of a defect cluster after absorbing a point defect of the same nature, 4. shrinkage of a defect cluster by the emission of a point defect of the same nature, 5. shrinkage of a defect cluster after absorbing a point defect of the opposite nature, and 6. loss of point defects to the thin-foil sample surface, considered as an inexhaustible sink.

The general form of these equations and the rate constants are in line with previous work in Ref. [8]. Although the equations are provided as developed for thermal diffusion reaction rates, in practice the rate constants are modified as explained in Section 2. The rate theory equations are given by

$$\frac{dC_{V_1}}{dt} = \chi G - K^S_{V_1} C_{V_1} - K^+_{V_1V_1} C_{V_1} C_{V_1} - \sum_{n=1}^{V-1} K^+_{V_1V_n} C_{V_1} C_{V_n} + K^+_{I_1V_2} C_{I_1} C_{V_2} - \sum_{n=1}^{I} K^+_{V_1I_n} C_{V_1} C_{I_n} + K^-_{V_2} C_{V_2} + \sum_{n=2}^{V} K^-_{V_n} C_{V_n} \quad (11)$$

$$\frac{\partial C_{V_n}}{\partial t} = K^+_{V_1,V_{n-1}} C_{V_1} C_{V_{n-1}} - K^+_{V_1V_n} C_{V_1} C_{V_n} + K^+_{I_1,V_{n+1}} C_{I_1} C_{V_{n+1}} - K^+_{I_1,V_n} C_{I_1} C_{V_n} + K^-_{V_{n+1}} C_{V_{n+1}} - K^-_{V_n} C_{V_n} \quad (12)$$

$$\frac{\partial C_{V_V}}{\partial t} = K^+_{V_1,V_{V-1}} C_{V_1} C_{V_{V-1}} - K^+_{I_1,V_V} C_{I_1} C_{V_V} - K^-_{V_V} C_{V_V} \quad (13)$$

$$\frac{\partial C_{I_1}}{\partial t} = \chi G - K^S_{I_1} C_{I_1} - K^+_{I_1,I_1} C_{I_1} C_{I_1} - \sum_{n=1}^{I-1} K^+_{I_1,I_n} C_{I_1} C_{I_n} + K^+_{V_1,I_2} C_{V_1} C_{I_2} - \sum_{n=1}^{V} K^+_{I_1,V_n} C_{I_1} C_{V_n} + K^-_{I_2} C_{I_2} + \sum_{n=2}^{I} K^-_{I_n} C_{I_n} \quad (14)$$

$$\frac{\partial C_{I_n}}{\partial t} = K^+_{I_1,I_{n-1}} C_{I_1} C_{I_{n-1}} - K^+_{I_1,I_n} C_{I_1} C_{I_n} + K^+_{V_1,I_{n+1}} C_{V_1} C_{I_{n+1}} - K^+_{V_1,I_n} C_{V_1} C_{I_n} + K^-_{I_{n+1}} C_{I_{n+1}} - K^-_{I_n} C_{I_n} \quad (15)$$

$$\frac{\partial C_{I_I}}{\partial t} = K^+_{I_1,I_{I-1}} C_{I_1} C_{I_{I-1}} - K^+_{V_1,I_I} C_{V_1} C_{I_I} - K^-_{I_I} C_{I_I} \quad (16)$$

where the C_{V_n} and C_{I_n} are the concentrations of vacancy and interstitial clusters of size n with C_{V_1} and C_{I_1} being the concentrations of single vacancies and interstitials. G is the displacement rate and χ is the surviving point defect fraction once the displacement cascade cools. The direct formation of clusters, $n > 1$, in the cascade is not considered.

The equations are truncated to a maximum interstitial cluster size of I atoms and a maximum vacancy cluster size of V vacancies. I and V are chosen to be large enough such that the concentration of defects of the maximum cluster size is negligible (i.e. so that defect clusters do not grow and end up piling-up in the largest cluster size). In the formulation used here, these values increase with temperature, where $I = 5000$ and $V = 500$ are used at 50 K and increase to $I = 50000$ and $V = 500$ at 500 K.

The term K^+ indicates the forward reaction rate constant between two defects and the term K^- indicates the backward reaction rate constant for dissociation of defects. The forward reaction constant is defined by the steady-state flux of defects to a stationary spherical sink with the form

$$K^+ = 4\pi r D \quad (17)$$

where D is the diffusion coefficient of the relevant defect and r is the interaction radius. The diffusion coefficient is of the typical form, $D = D_0 \exp(-E_m/k_B T)$, where D_0 is the diffusion prefactor. The interaction radius is taken as the sum of the reactants' physical radii and a recombination radius, r_c. For the reactions involving two diffusing species, the diffusion coefficients of the two reactants are added. Reaction rates involving two interstitial type defects were multiplied by an interstitial bias of 1.05 to account for their greater elastic interaction than vacancies [10].

The backward reaction (emission of defects from a defect cluster) is defined as

$$K^- = \frac{K^+}{\Omega} \exp\left(\frac{-E_b}{k_B T}\right) \quad (18)$$

where Ω is the atomic volume, E_b is the binding energy of the defect to the cluster in question and k_B is the Boltzmann constant. Following Soneda and De La Rubia, the binding energy is given the form [11]

$$E_b(n) = A - B\left[n^{2/3} - (n-1)^{2/3}\right] \quad (19)$$

where A and B are constants. These constants are found by considering that binding energy tends toward the point defect formation energy at large sizes, and the binding energies for di-interstitials and di-vacancies are as calculated in Ref. [8]. In particular,

$$A = E_f$$

and

$$B = \frac{E_f - E_b(2)}{2^{2/3} - 1}$$

are used in this work. $E_b(2)$ is the binding energy of the di-interstitial and di-vacancy.

Due to the small thickness of the TEM samples used during in-situ irradiation, the surfaces act as strong sinks for mobile defects. The rate theory equations are not developed here with explicit spatial dependence to model that behavior. Loss of defects to the surface is instead expressed through another rate constant, K^S. A parabolic concentration profile of migrating defects within the foil is assumed with the maximum concentration at the center of the sample and zero concentration at the two surfaces. The total flux of defects to the two surfaces was then calculated as a function of the average defect concentration. When divided by the sample thickness, this represents the average rate density of defect loss to the sample surfaces. The rate density of defects lost to surfaces is

$$K^S C \quad (20)$$

where

$$K^S = \frac{12D}{L^2} \quad (21)$$

and L is equal to the thickness of the sample.

4. Results and discussion

The addition of the thermal spike model to reaction rate constants is discussed first. The thermal diffusion reaction rate at which interstitials cluster to form di-interstitials is given by

$$(\text{rate})_{\text{diff}} = K_{I_1I_1} C_{I_1} C_{I_1} = \left[8\pi(2r_I + r_C) C_{I_1} C_{I_1} D_0\right] \exp\left(\frac{-E_{mi}}{k_B T}\right) \quad (22)$$

where the term in square brackets is equivalent to A in Eq. (3). Calculation of the "athermal" thermal spike reaction rate and total reaction rate is as shown in Section 2. Dropping the terms for interstitial concentration, C_{I_1}, from each leaves only the rate constants which are shown in Fig. 2 as functions of temperature. The athermal reaction rate dominates at low temperatures, the thermal diffusion reaction rate dominates at high temperatures, and a continuous transition is observed between the two at 176 K where the two are equal. This temperature is as shown in

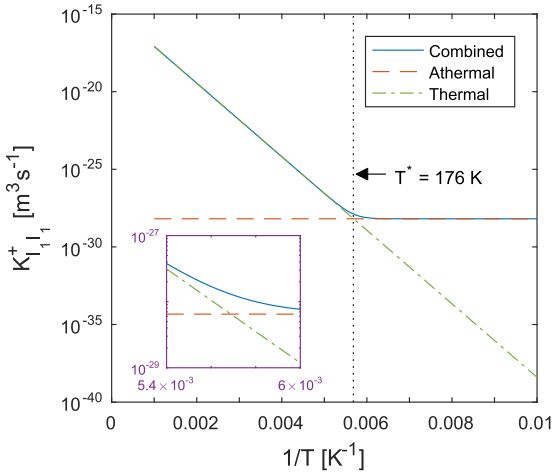

Fig. 2. The thermal diffusion, "athermal" thermal spike, and combined reaction rate constants as functions of temperature for the reaction of two interstitials forming an interstitial cluster. The athermal-thermal equivalence temperature is marked and corresponds to the interstitial migration energy, 0.47 eV, in Fig. 1.

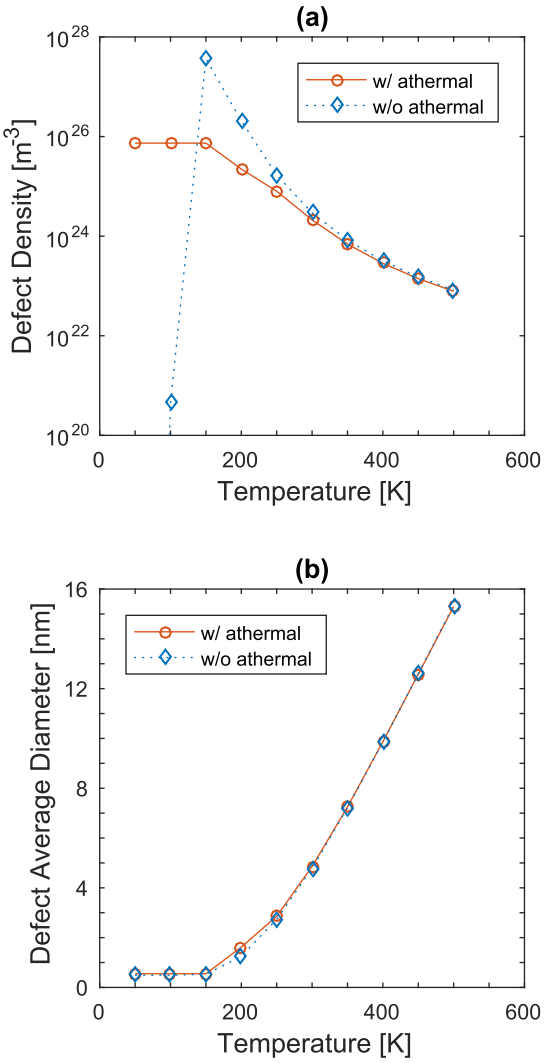

Fig. 3. Rate theory simulation results showing (a) defect density and (b) average diameter of all interstitial clusters, di-interstitials and larger, using only thermal diffusion controlled reaction rates and with the addition of "athermal" thermal spike reaction rates at 1 dpa.

Fig. 1 and corresponds to the reaction energy of 0.47 eV, the migration energy of interstitials. It is clear that the addition of the thermal spike reaction rate avoids the precipitous drop in reaction rates at low temperature that happens when only thermal diffusion controlled reactions at the ambient temperature are considered.

The system of rate theory cluster dynamics equations with additional "athermal" thermal spike reaction rates was solved for temperatures ranging from 50 K to 500 K. The parameters used in the model are shown in Table 1. References for values are provided when available, but otherwise physically reasonable values of the parameters were chosen. An adaptive time step algorithm was used as described in Ref. [12], where each time step was accepted if the estimated relative truncation error was below 10^{-3}. Each time step was solved iteratively to a relative convergence criteria of less than 10^{-5}. The simulation data is aggregated into defect cluster average diameter and density for easy presentation. It should be noted that only the data for interstitial clusters is shown; it was found that vacancy clusters never grew large enough to be visible in TEM ($>$ 1.5 nm diameter).

Fig. 3 shows the density and average diameter of all interstitial clusters using only thermal diffusion controlled reaction rates and with the addition of "athermal" thermal spike reaction rates. The nucleation and growth of interstitials is controlled mainly by the interstitial migration energy, 0.47 eV. From Fig. 1 it is shown that the transition from athermal to thermal regimes occurs at 176 K for this reaction energy. At temperatures much greater than this temperature, the simulations produce similar results, as seen with the overlapping lines above 300 K in Fig. 3. In the simulation below this temperature, the reaction rates exponentially fall with decreasing temperature in the absence of the additional thermal spike model. While the simulation with athermal reactions levels off below 175 K, the model without athermal reactions behaves erratically. First, the density increases significantly as compared to the other model[1] before becoming numerically insignificant as the reaction rates approach zero and defects cannot cluster.

A simulation at 50 K with the "athermal" thermal spike model included is compared to experimental values in Fig. 4. Only defects with diameter greater than 1.5 nm (representing the minimum defect size visibility in the TEM) are shown. The experimental values at 673 K, 873 K and 1073 K are reproduced from Ref. [4]. Additionally, a single point was added from the in-situ irradiation of $ZrC_{0.9}$.[2] Overall, the results of the calculation exhibit several desirable attributes which compare well with the experimental results:

1. There is an incubation period of approximately 0.5 dpa before visible defects can be seen.
2. The defect density saturates after a few dpa.
3. The defect diameter does not grow to large sizes.
4. The magnitude of the defect density, approximately 10^{23} m^{-3} after saturation, is similar to experiment.

More importantly, without the addition of the athermal reaction rates, no TEM visible defects would have been formed. The

[1] This behavior is reproduced in large part by disabling dissociation reactions in the thermal spike model.

[2] This data was not quantified previously because the thickness of this sample was not measured. The density error bars at 50 K represent the range of thicknesses previously measured in other samples. Also, the diffraction condition is a semi-weak $g = 220$ dark-field, as opposed to the $g = 002$ condition that was used for the other data points.

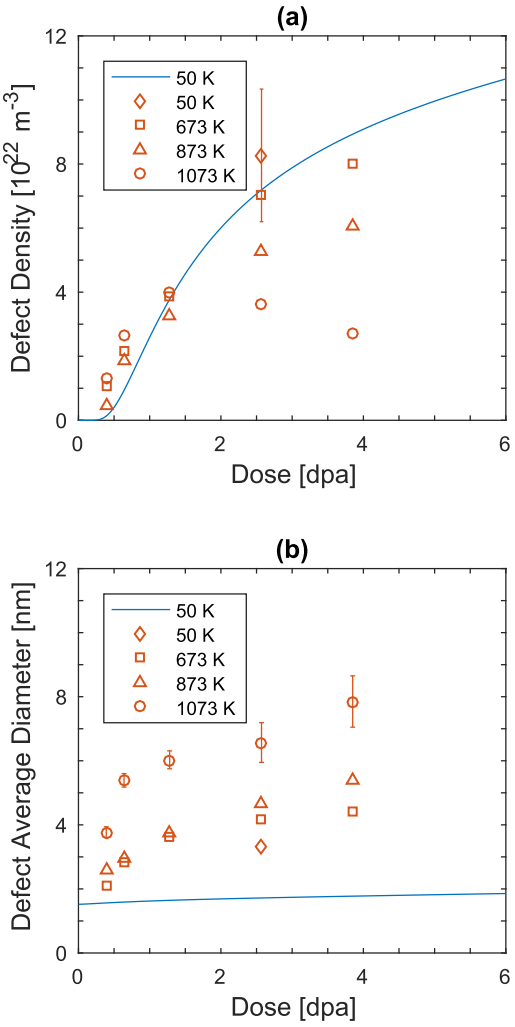

Fig. 4. Rate theory simulation results for (a) defect density and (b) average diameter at 50 K (line) and comparison to experimental values obtained from in-situ irradiation (markers). The rate theory results show only data for defects that are expected to be visible (> 1.5 nm diameter). The error bars are shown only for the data set with the largest error.

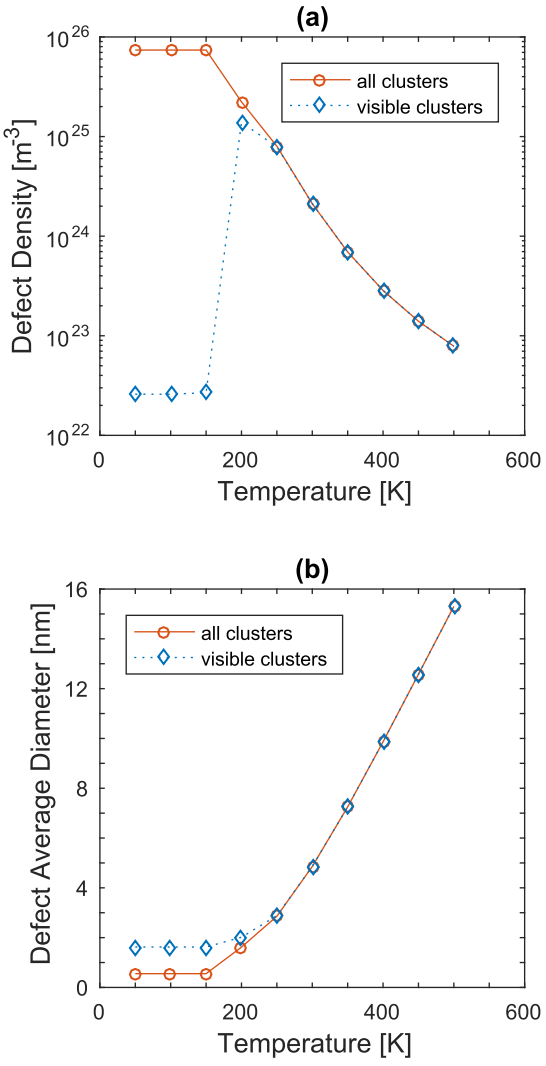

Fig. 5. Rate theory simulation results showing (a) defect density and (b) average diameter of all interstitial clusters (di-interstitials and larger) and visible interstitial clusters (greater than 1.5 nm diameter) with the additional "athermal" thermal spike reaction rates at 1 dpa.

addition of the athermal reaction process produces better results that are of the same order of magnitude as experiment at low temperature. This process would be expected to have similar effect for very high dose rate situations as well.

The rate theory cluster dynamics modeling results for average defect diameter and density as a function of temperature and dose are shown in Fig. 5 for both all and only visible interstitial clusters using the "athermal" thermal spike reaction rates. The model produces results that are independent of temperature from 50 K up to 150 K, demonstrating that the athermal mechanisms are still dominant up to 150 K. By 200 K, interstitial diffusion has become thermally activated and surpassed the athermal contribution. The break-even temperature for thermal vs. athermal interstitial migration is 176 K, so the reactions involving interstitials have increased in rate while other reactions with higher activation energy have not increased significantly from the athermal regime. This results in interstitial clusters growing more quickly. Since many of the defects were below the visibility criteria at 50 K, the increased loop growth greatly increases the visible defect density while the total cluster density decreases. Further increases in temperature above 200 K result in decreasing defect density and increasing defect average diameter. These trends match those observed from experiments.

However, the rate at which the model's prediction of defect density and diameter changes with temperature is much higher than observed experimentally. The in-situ measurements of defect size and density did not change by more than an order of magnitude over temperatures ranging from 50 K to 1073 K, in contrast to the model calculations which show much larger changes in defect density and size with temperature. This occurs because interstitial migration, which activates first at 0.47 eV, dominates the other reactions which leads to significant defect growth as the temperature increases. All other processes activate at energies that are too high for the temperature range of 50 K to 1073 K. For example, vacancy diffusion, with migration energy 5.44 eV, does not thermally activate until 1783 K (see Fig. 1). The experimental results which begin to show defect growth in the range of 300 K to 473 K would indicate an activation energy in the range of 0.8 eV to 1.4 eV based on the athermal model.

From these results, the diffusion of interstitials and vacancies alone cannot explain the full irradiation behavior of ZrC, and additional reactions would need to be added for a complete model. While it has not been studied thoroughly in ZrC, the direct production of defect clusters has been observed in molecular dynamics simulations of displacement cascades [13] and could occur during irradiation. This would reduce the production of mobile defect

clusters and could alter nucleation kinetics. Additionally, the relations used to calculate binding energy of point defects to defect clusters may not be accurate for all defect sizes. Finally, it is easy to imagine that small defect clusters are also mobile, and, because they are below the resolution limit of TEM, would not be observed during the in-situ experiment. Further study of the direct production of defect clusters in displacement cascades and the formation and migration energy of defect clusters is required to improve the accuracy of rate theory modeling of radiation damage in ZrC.

This work shows how a thermal spike model can be applied to generate athermal reaction rates for rate theory cluster dynamics simulations of microstructure evolution during irradiation. Using physical parameters and a simple model, the simulation in the athermal regime matched well with experiment. The same procedure outlined in this work can be applied to any thermally activated process to calculate athermal reaction rates and can therefore be applied to more complicated models. The thermal spike model is most applicable to low temperature or high damage rate irradiation conditions, and simulation of ion irradiation microstructure evolution may benefit the most from its use. Several simplifications were used in the derivation of the thermal spike model, including spherical/cylindrical geometry symmetry and constant defect density in the vicinity of the thermal spike. The impact of these simplifications should be assessed in future work, possibly using molecular dynamics simulations of displacement cascades.

5. Conclusion

A thermal spike model was formulated to calculate athermal reaction rates to address the low temperature deficiency of classical rate theory models. The thermal spike reaction rate was added to a simple rate theory cluster dynamics model of radiation damage and applied to in-situ irradiation results of ZrC. The resulting rate theory model can be applied at all temperatures and overcomes the fact that most thermally activated processes do not occur at cryogenic temperatures. The results of the calculation with the athermal model showed several qualitative improvements over the purely thermal model in comparison to experimental observations. The results of the model, however, changed more rapidly with temperature than experiment, indicating that further work is needed to develop a model that works at all temperatures. In such circumstances the thermal spike model can be successfully used to augment rate theory modeling to predict irradiation damage at low temperatures.

Acknowledgments

This work was completed under funding by the U.S. Department of Energy's Nuclear Engineering University Program project number 10-679 and Integrated Research Project DE-NE0000639. We thank Ming-Jie Zheng, Izabela Szlufarska, and Dane Morgan for their insightful discussions on microstructure evolution in ZrC.

References

[1] A. Brailsford, R. Bullough, J. Nucl. Mater. 44 (1972) 121–135, http://dx.doi.org/10.1016/0022-3115(72)90091-8.
[2] M.R. Hayns, J. Nucl. Mater. 56 (1975) 267–274, http://dx.doi.org/10.1016/0022-3115(75)90042-2.
[3] D. Xu, B.D. Wirth, M. Li, M.A. Kirk, Acta Mater. 60 (2012) 4286–4302, http://dx.doi.org/10.1016/j.actamat.2012.03.055.
[4] C.J. Ulmer, A.T. Motta, M.A. Kirk, J. Nucl. Mater. 466 (2015) 606–614, http://dx.doi.org/10.1016/j.jnucmat.2015.08.009.
[5] M.-J. Zheng, I. Szlufarska, D. Morgan, J. Nucl. Mater. 457 (2015) 343–351, http://dx.doi.org/10.1016/j.jnucmat.2014.11.059.
[6] G.H. Vineyard, Radiat. Eff. 29 (1976) 245–248, http://dx.doi.org/10.1080/00337577608233050.
[7] J.F. Ziegler, M.D. Ziegler, J.P. Biersack, Nucl. Instrum. Methods Phys. Res., Sect. B 268 (2010) 1818–1823, http://dx.doi.org/10.1016/j.nimb.2010.02.091.
[8] S. Pellegrino, J.-P. Crocombette, A. Debelle, T. Jourdan, P. Trocellier, L. Thomé, Acta Mater. 102 (2016) 79–87, http://dx.doi.org/10.1016/j.actamat.2015.09.004.
[9] S. Kim, I. Szlufarska, D. Morgan, J. Appl. Phys. 107 (2010) 053521, http://dx.doi.org/10.1063/1.3309765.
[10] W. Wolfer, J. Comput. Aided Mater. Des. 14 (2007) 403–417, http://dx.doi.org/10.1007/s10820-007-9051-3.
[11] N. Soneda, T.D. De La Rubia, Philos. Mag. A 78 (1998) 995–1019, http://dx.doi.org/10.1080/01418619808239970.
[12] D. Kavetski, P. Binning, S.W. Sloan, Int. J. Numer. Meth. Eng. 53 (2002) 1301–1322, http://dx.doi.org/10.1002/nme.329.
[13] L.V. Brutzel, J. Crocombette, Nucl. Instrum. Methods Phys. Res., Sect. B 255 (2007) 141–145, http://dx.doi.org/10.1016/j.nimb.2006.11.048.
[14] Y. Katoh, G. Vasudevamurthy, T. Nozawa, L.L. Snead, J. Nucl. Mater. 441 (2013) 718–742, http://dx.doi.org/10.1016/j.jnucmat.2013.05.037.